Cancer Immunology, Immunotherapy (2019) 68:2005–2014
https://doi.org/10.1007/s00262-019-02428-3

ORIGINAL ARTICLE

Serum very long-chain fatty acid-containing lipids predict response to immune checkpoint inhibitors in urological cancers

Andreas Mock[1] · Stefanie Zschäbitz[1] · Romy Kirsten[2] · Matthias Scheffler[3] · Barbara Wolf[3] · Christel Herold-Mende[4] · Rebecca Kramer[1] · Elena Busch[1] · Maximilian Jenzer[1] · Dirk Jäger[1] · Carsten Grüllich[1,5]

Received: 23 March 2019 / Accepted: 1 November 2019 / Published online: 7 November 2019

Abstract

Checkpoint inhibitors (CPI) have significantly changed the therapeutic landscape of oncology. We adopted a non-invasive metabolomic approach to understand immunotherapy response and failure in 28 urological cancer patients. In total, 134 metabolites were quantified in patient sera before the first, second, and third CPI doses. Modeling the association between metabolites and CPI response and patient characteristics revealed that one predictive metabolite class ($n = 9/10$) were very long-chain fatty acid-containing lipids (VLCFA-containing lipids). The best predictive performance was achieved through a multivariate model, including age and a centroid of VLCFA-containing lipids prior to first immunotherapy (sensitivity: 0.850, specificity: 0.825, ROC: 0.935). We hypothesize that the association of VLCFA-containing lipids with CPI response is based on enhanced peroxisome signaling in T cells, which results in a switch to fatty acid catabolism. Beyond use as a novel predictive non-invasive biomarker, we envision that nutritional supplementation with VLCFA-containing lipids might serve as an immuno sensitizer.

Keywords Cancer immunotherapy · Cancer metabolomics · Renal cell carcinoma · Urothelial cancer

Electronic supplementary material The online version of this article (https://doi.org/10.1007/s00262-019-02428-3) contains supplementary material, which is available to authorized users.

Andreas Mock and Stefanie Zschäbitz have contributed equally to this work.

✉ Carsten Grüllich
carsten.gruellich@med.uni-heidelberg.de

[1] Department of Medical Oncology, National Center for Tumor Diseases (NCT) Heidelberg, Heidelberg University Hospital, Im Neuenheimer Feld 460, 69120 Heidelberg, Germany

[2] Liquid Biobank, National Center for Tumor Diseases (NCT) Heidelberg, Heidelberg University Hospital, Heidelberg, Germany

[3] BIOCRATES Life Sciences AG, Innsbruck, Austria

[4] Division of Experimental Neurosurgery, Department of Neurosurgery, Heidelberg University Hospital, Heidelberg, Germany

[5] Present Address: Department of Urology, Dresden University Hospital, Gustav Carus Fetscherstr. 74, 01307 Dresden, Germany

Abbreviations

CI	Confidence interval
CPI	Checkpoint inhibitor
CR	Complete remission
FAO	Fatty acid oxidation
FDG-PET	Fluorodeoxyglucose positron emission tomography
GLC	Glucose
GPL	Glycerophospholipid
HR	Hazard ratio
LCFA	Long-chain fatty acid
LMM	Linear mixed effects model
LOD	Limit of detection
MS	Mass spectroscopy
NMR	Nuclear magnetic resonance
PC	Phosphatidylcholine
PD	Progressive disease
PPAR-α	Peroxisome proliferation-activated receptor α
PR	Partial remission
RCC	Renal cell carcinoma
ROC	Receiver operating characteristic
SD	Stable disease
SLC27A2	Solute carrier family 27 member 2 gene
sGPL	Saturated GPL

SM	Sphingomyelin
SVM	Support vector machine
TCGA	The Cancer Genome Atlas
TMB	Tumor mutational burden
tSNE	T-distributed stochastic neighbor embedding
UC	Urothelial carcinoma
uGPL	Unsaturated GPL
VLCFA	Very long-chain fatty acid

Introduction

Metabolomics aims to characterize and quantify metabolites in organic liquids or tissues. The metabolome is influenced by genetics and environmental factors such as exercise, smoking, or nutrition [1]. There is increasing interest in the use of comparative metabolomic profiling in cancer research. Most published genomic and transcriptomic landscapes do not adequately explain disease phenotypes or predict therapy responses. The emerging hallmarks of cancer metabolism include dysregulation of glucose and amino acid uptake, opportunistic uptake of metabolites from the microenvironment, biosynthesis and NADPH production through glycolysis and the citrate acid cycle, an increased need for nitrogen, and gene dysregulation caused by metabolites and other interactions with the microenvironment [2]. In fact, the fluorodeoxyglucose positron emission tomography (FDG-PET) technique uses this characteristic of altered glucose metabolism to routinely detect tumor tissues [3]. Metabolomic signatures from serum or urine samples have been identified as prognostic markers for various tumor entities and as markers for early disease detection; however, they are still not part of routine clinical practice [4–7].

The most common technologies used to measure metabolites are mass spectroscopy (MS), enzyme-linked immunosorbent assay (ELISA), and nuclear magnetic resonance (NMR) spectroscopy. Throughput, sensitivity, depth of coverage, and cost vary significantly depending on which method is used. Untargeted metabolomics describes the analysis of all measurable analytes in a given sample, while targeted metabolomics involves target-oriented identification and absolute qualification of known metabolites. The metabolite portfolio encompasses the following: amino acids; vitamins; bile acids; short-chain, medium-chain, and long-chain fatty acids (FA); and lipids such as (acyl-) carnitines, glycerophospholipids (GPL), sphingolipids, or lipid precursors. Long-chain fatty acids (LCFA) consist of a carboxylic acid with an aliphatic chain of 14–21 carbons, while the tail of very long-chain fatty acids (VLCFA) has at least 22 carbons. It has been reported that VLCFA and LCFA induce necroptosis and inflammatory signals through a variety of mechanisms [8, 9]. VLCFA, unlike LCFA, are metabolized in peroxisomes, rather than in the mitochondria. In the peroxisomes, they activate peroxisome proliferation-activated receptor α (PPARα) signaling, and thus control pivotal genes involved in lipid metabolism [10].

Despite tumor metabolism being a promising area of research, immunometabolism, which is the interaction between the immune system and metabolism, has received special research focus in the age of cancer immunotherapy [11]. Deviant metabolites of tumor cells affect their microenvironment. For example, the activity and function of T cells are influenced by restriction of glucose availability or excessive lactate excretion by tumor cells [12, 13].

In recent years, checkpoint inhibitors (CPI) have been added to the treatment armamentarium for metastatic renal cell carcinoma (RCC) and urothelial cancer (UC). In UC, the use of CPI for first-line treatment is restricted to programmed cell death ligand 1 (PD-L1) positive tumors. The combination of nivolumab and ipilimumab as first-line treatment for intermediate and high-risk RCC was FDA-approved in June 2018 and EMA-approved in February 2019 following the results of the KEYNOTE-052 trial [14]. Anti-PD1 (programmed cell death protein 1) and anti-PD-L1 antibodies can be applied as second-line agents independent of RCC risk profile and UC PD-L1 status.

Positive PD-L1 expression [15], tumor mutational burden (TMB) [16], microsatellite status, and tumor infiltrating lymphocytes (TILs) [17] are candidates for response prediction to CPI treatment. The predictive power of these markers; however, varies greatly between studies and cancer types. Differing methodologies and reagents used for biomarker testing also add to the confusion.

There is emerging data that metabolomic profiles might predict the response to treatment with checkpoint inhibitors. In patients with melanoma and RCC treated with nivolumab, levels of kynurenine and adenosine differed significantly between responders to CPI and non-responders [18, 19]. We aimed to determine whether metabolites are predictive of treatment response in patients with UC or RCC undergoing CPI treatment.

Materials and methods

Study sample

Consent to biobank blood samples from patients with metastatic RCC or UC who underwent CPI treatment at Heidelberg University Hospital was obtained starting from 24.02.2016. Paired serum samples were collected prior to the first (28 patients), second (18 patients), and third doses (16 patients) of CPI treatment. These were then aliquoted and stored at − 80 °C until used. Medical records for all patients were accessed through electronic patient charts. Clinical data were prospectively collected from the date of

patient consent. Clinical parameters assessed included histopathologic diagnosis, tumor stage and grading, location of metastases, type and duration of and response to prior treatment, type and duration of CPI treatment, first and best response to CPI treatment, and side effects of CPI treatment. Overall survival (OS) was calculated from the date of the first CPI dose to the date of death or last follow up (last assessed on 13.02.2019). Duration of CPI treatment was included as a secondary endpoint. Responders to CPI treatment were defined as those who achieved complete remission (CR), partial (PR) remission, or stable (SD) disease. Patients with progressive disease (PD) were defined as non-responders to CPI. Response was evaluated using RECIST 1.1 criteria.

Metabolomic analysis and data preprocessing

Mass spectrometric metabolite quantification was performed at BIOCRATES Life Sciences AG, Innsbruck, Austria. All serum samples were analyzed using the Absolute*IDQ*® p180 kit (BIOCRATES Life Sciences AG, Innsbruck, Austria), which enables the absolute quantification of 188 metabolites using internal standards. Sample analysis was performed using MS technology (liquid chromatography MS for analysis of amino acids and biogenic amines, and flow injection analysis MS for analysis of lipids, acylcarnitines, and hexose) as previously described [20]. The limit of detection (LOD) was set to three times the median signal detected in the zero control samples as previously described [21]. Metabolites were excluded when measurements were below 20% of the LOD. The total number of metabolites available following data cleaning was 134 (9 acylcarnitines, 21 amino acids, 10 biogenic amines, 1 hexose, 14 saturated GPLs, 14 sphingolipids, 65 unsaturated GPLs). To calculate the fraction of lipid isomers containing VLCFAs, we used the annotation of potential isobaric and isomeric lipid species measured with the Absolute*IDQ*® p180 kit provided by BIOCRATES Life Science AG. Measurements were log2-transformed prior to statistical analyses.

Transcriptome and survival analysis in TCGA data

Gene-level RNA-sequencing count data for the six acyl-CoA synthetases that metabolize VLCFAs (SLC27A1-6) were downloaded from *The Cancer Genome Atlas* (TCGA) for RCC ($n = 587$) and UC ($n = 427$) via the curatedTCGAData R package [22]. Updated clinical data were obtained from the Supplemental Table S1 of a recently published pan-cancer TCGA manuscript [23]. For Kaplan–Meier curves, logarithmic count data were dichotomized into a high-expression and low-expression groups according to the count value cut-off within the interquartile range with the lowest p value in a cox-proportional hazard model.

Statistical analyses

All statistical analyses were conducted using R software (R version 3.4.2; www.r-project.org). Data were stored within a 'SummarizedExperiment' class object enabling coordinated representation of the metabolomic data and associated metadata. Heatmaps were produced using the *ComplexHeatmap* package, and boxplots and scatter plots were generated using the *ggplot2* package. T-distributed stochastic neighbor embedding (tSNE) was performed using the *Rtsne* R package. Multivariate linear mixed effects modeling was employed to determine metabolites associated with therapy response. Linear mixed effects models (LMMs) also include random effects (between patient variation), in addition to fixed effects (therapy response and patient age). The *nlme* package offers the functionality of LMMs within R [24]. We compared the predictive performance of patient age and median concentration (i.e., the centroids) of the VLCFA-containing lipids belonging to cluster 1 and cluster 2 (compare Fig. 3c) in univariate and multivariate models. We applied tenfold cross validation to each model, repeated ten times, to compensate for overfitting. In addition, we used a linear (logistic regression) and a non-linear (support vector machine [SVM]) approach. The predictive modeling was performed with the *caret* R package. All presented p values are not adjusted for multiplicity. A p value of < 0.05 was considered statistically significant. Original data and material are available upon request from the corresponding author.

Results

Study design and patient cohort

Serum samples were collected from tumor patients before the first, second, and third doses of an immune checkpoint inhibitor (time points T1, T2, T3; Fig. 1a). A total of 134 metabolites were quantified (Fig. 1b). The study cohort included 28 patients (Supplementary Table 1); 25 (89.3%) had RCC with predominant clear cell characteristics, two (7.1%) had UC, and one patient (3.6%) was diagnosed with both UC and clear cell RCC. All patients received treatment with nivolumab, except one RCC patient treated with atezolizumab and bevacizumab. The median age of the cohort was 64 years (range 41–79 years); 23 patients were male (82.1%) and five were female (17.9%). Individual clinicopathological characteristics are summarized in Supplementary Table 2. The number of treatment lines was balanced between responders and non-responders. Five patients in the responders group received nivolumab as fourth-line or fifth-line treatment.

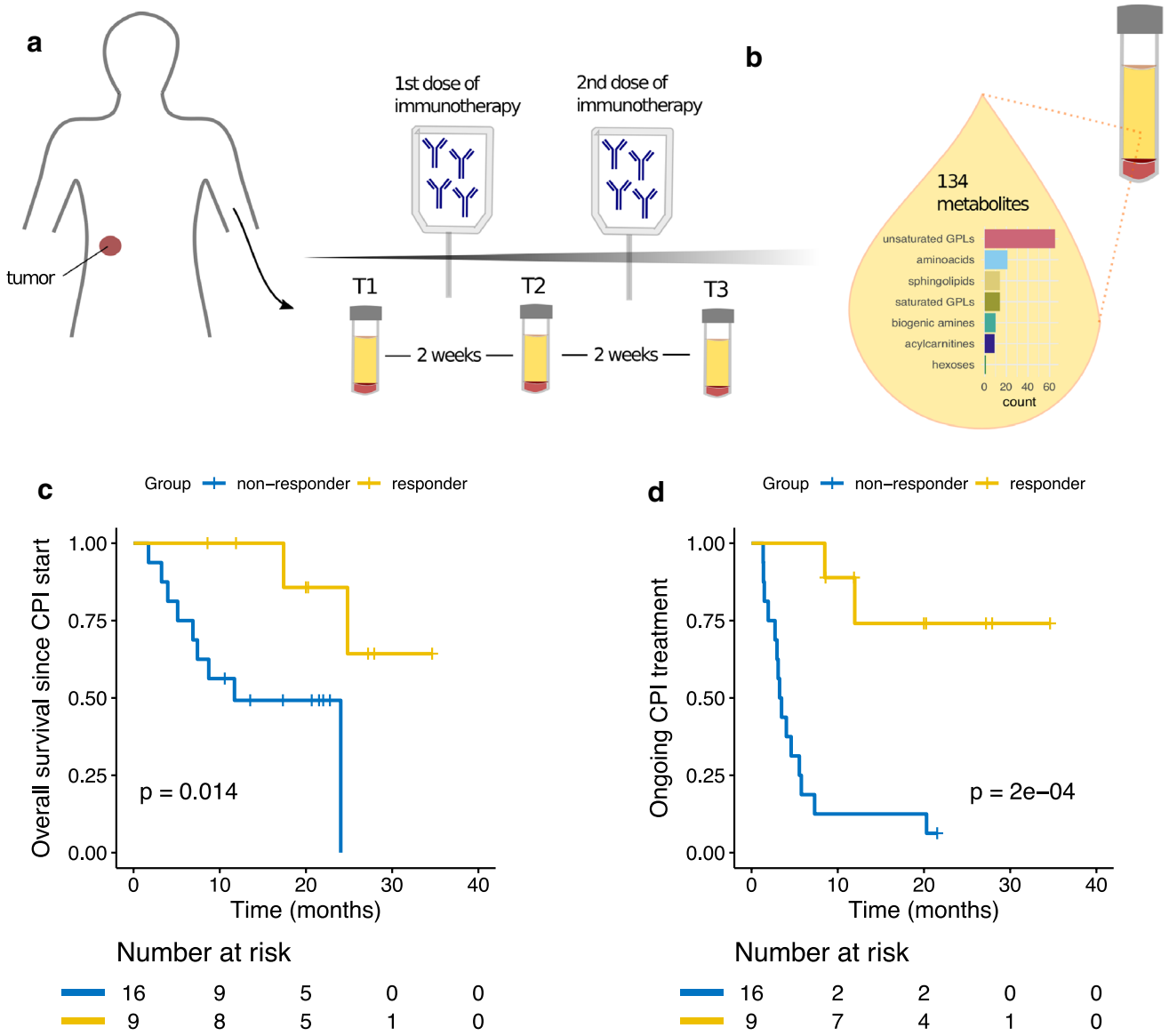

Fig. 1 Graphical abstract of study design and survival analysis in study cohort. **a** Serum was collected from patients with tumors before the first, second, and third doses of immune checkpoint inhibitor therapy. **b** A total of 134 metabolites was quantified using the AbsoluteIDQ® p180 kit (BIOCRATES Life Sciences AG, Innsbruck, Austria). **c** Kaplan–Meier curve of overall survival since CPI initiation stratified by the best response to CPI. **d** Kaplan–Meier curve of duration of CPI treatment stratified by the best response to CPI

The best response to treatment was PR in four patients (14.3%), SD in eight patients (28.6%), and PD in 15 patients (53.6%). No CR was observed. The overall survival from CPI initiation was significantly higher in CPI responders compared to non-responders (Fig. 1c, $p = 0.014$, HR = 0.11 [95% CI 0.01–0.88]). The duration of CPI treatment was also longer in CPI responders compared to non-responders (Fig. 1d, $p = 2 \times 10^{-4}$, HR = 0.09 [95% CI 0.02–0.42]).

Unsupervised analysis of serum metabolomes

We first visualized the metabolome-wide variance in the dataset by means of t-distributed stochastic neighbor embedding (tSNE). The tSNE plot revealed greater variance in metabolomic measurements between patients than within the same patient over time (Fig. 2a). The 134 metabolites analyzed were assigned to one of seven metabolite classes (hexoses, amino acids, sphingolipids, unsaturated GPLs,

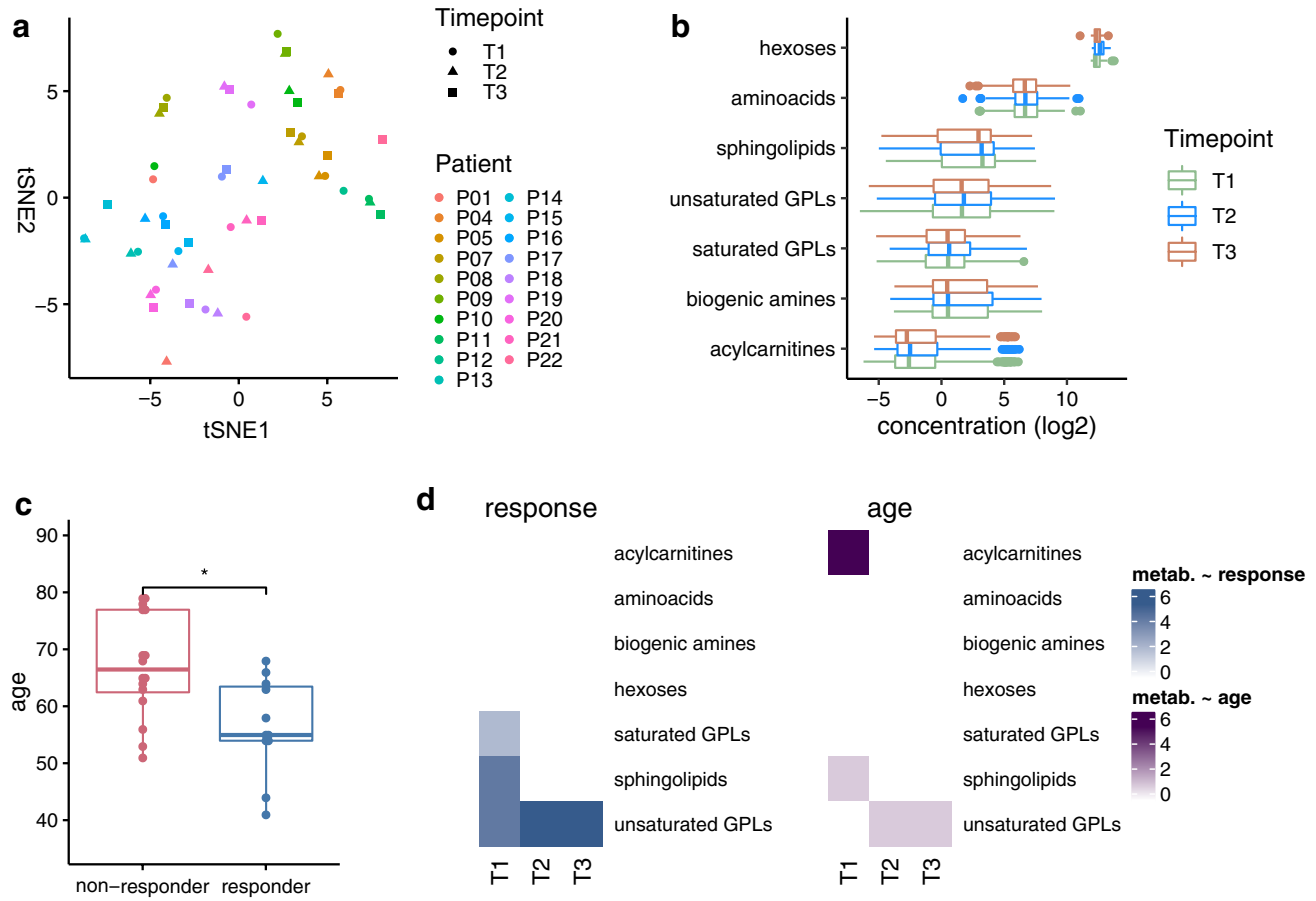

Fig. 2 Unsupervised and supervised comparative analyses of metabolomes. **a** tSNE plot comparing the metabolome of all patients at the three different time points. **b** Distribution of measured concentrations per metabolite class stratified by the three different time points. **c** Boxplot of patient age stratified by immunotherapy response ($p = 0.013$). **d** Summary heatmaps illustrating the number of significant metabolites associated with response and age stratified by metabolite class ($p < 0.05$)

saturated GPLs, biogenic amines, and acylcarnitines). The average concentration calculated for these classes showed that the pool of metabolites remained constant over the three measured time points (Fig. 2b).

Metabolites associated with response to immunotherapy

Known prognostic factors were considered in our patient cohort before comparing the metabolomes of immunotherapy responders and non-responders. In line with published studies [25], responders to immunotherapy were significantly younger than non-responders in our study (Fig. 2c). Hence, we applied a multivariate modeling approach which revealed differentially abundant metabolites in the response groups independent of patient age. The heatmap in Fig. 2d illustrates the number of metabolites significantly associated with response and patient age stratified for the three different time points. The highest number of metabolites associated with response was identified before the first immunotherapy dose (time point T1).

Very long-chain fatty acid-containing lipids are predictive of immunotherapy response

The vast majority of metabolites (9/10) associated with response to immunotherapy at T1 were very long-chain fatty acid-containing lipids (VLCFA-containing lipids; Table 1). This observation was highlighted when plotting the fraction of potential isomers containing VLCFAs for every lipid over the response p value (Fig. 3a). We also observed that their predictive performance continuously decreased from T1 to T3 (Fig. 3b). To corroborate the role of VLCFAs, we compared the fraction of potential VLCFA-containing lipids with the length of the two fatty acids of all unsaturated GPLs (uGPLs). This yielded a strong correlation (Supplementary Fig. 1, $r = 0.90$). uGPLs were used for this comparison, as they were the largest group of lipids in the dataset (65 metabolites). uGPLs with VLCFAs showed more correlation

Table 1 Metabolites associated with immunotherapy response independent of patient age ($p < 0.05$)

Metabolite	Class	log2 (fold-change)	p value	∑ FA chain length	Isomers ≥ 22C
PC aa C38:0[a]	sGPL	0.488128877	0.027	38	7/12
PC aa C42:0	sGPL	0.566755571	0.031	42	3/4
PC aa C42:2	uGPL	0.437668994	0.013	42	6/6
PC ae C40:6	uGPL	0.420863679	0.047	40	4/6
PC ae C42:3	uGPL	0.615033724	0.005	42	6/8
PC ae C44:6	uGPL	0.512514563	0.024	44	2/2
SM (OH) C22:1	Sphingolipid	0.444489484	0.047	22	4/4
SM C24:1	Sphingolipid	0.461333761	0.025	24	2/2
SM C26:1	Sphingolipid	0.517973234	0.029	26	1/1
SM C20:2	Sphingolipid	0.4872320	0.039	20	0/2

∑ FA chain length = sum of fatty acid chain length; isomers ≥ 22C = fraction of potential isomeric lipids containing at least one fatty acid with a chain length greater than or equal to 22

sGPL saturated glycerophospholipid, *uGPL* unsaturated glycerophospholipid, *PC* phosphatidylcholine, *SM* sphingomyelin

[a]PC aa C38:0 has two potential isomers with unsaturated fatty acids

between each other than with uGPLs containing medium-chain or short-chain fatty acids (Supplementary Fig. 2). The nine predictive VLCFA-containing lipids revealed two distinct anti-correlated clusters (Fig. 3c). The first cluster comprised three sphingomyelins (SM) and the second cluster included six phosphatidylcholines (PC).

Predictive modeling of therapy response

Due to the lack of an independent validation cohort, we performed rigorous predictive modeling in our patient cohort to estimate the predictive performance of the VLFCA-containing lipids. We applied tenfold cross validation to each model, which was repeated ten times, to compensate for overfitting. In addition, we used a linear (logistic regression) and a non-linear (support vector machine; svm) approach. The best performance was achieved by the multivariate logistic regression model which included age and centroid 2, corresponding to the median concentration of the six phosphatidylcholines presented in cluster 2 of Fig. 3c (sensitivity: 0.850, specificity: 0.825, ROC: 0.935; Fig. 3d, Suppl. Table 3).

Prognostic activation of very long-chain acyl-CoA synthetase SLC27A2 in urological tumor tissues

Based on the predictive performance of VLCFA in patient sera, we questioned their role in the metabolism of urological tumor tissues. Due to the lack of metabolic measurements in tissue samples, we investigated the expression of VLCFA metabolism-related genes in clear cell RCC and bladder UC of *The Cancer Genome Atlas* (TCGA). VLCFAs are metabolized in the peroxisomes, where they support fatty acid catabolism (Fig. 4a). Before VLCFAs can be degraded via the chain-shortening peroxisomal β-oxidation, they must be activated by acyl-CoA synthetases (ACS) (Fig. 4b). The human genome encodes six ACS family genes that metabolize VLCFAs and are designated SLC27A1-6. Comparative transcriptomics revealed a significant prognostic value for the expression of SLC27A2 in both the TCGA RCC ($p < 0.0001$, Fig. 4c) and UC cohort ($p = 0.00021$, Fig. 4d).

Discussion

The field of immunooncology offers a fascinating new perspective for the treatment of cancer. The immune system is, however, extremely complex and tightly regulated and predictive biomarkers for CPI response are currently one of the most investigated areas of research. The expression of PD-L1, the target of PD-L1/PD1-directed therapies, appears to be of limited predictive value especially in genitourinary tumors. While response rates are higher in PD-L1 positive tumors, PD-L1 negative tumors also respond to these therapies, albeit at lower rates. TMB has been proposed as another potential biomarker as it may be a surrogate for neoantigen expression-driven immunogenicity; however, data on this remain inconclusive. A correlation between response and tumors high in TMB has been described for urothelial cancer [14], but not renal cell cancer [26].

We adopted a longitudinal non-invasive metabolomic approach to reveal new insights regarding the mechanisms for immunotherapy response as well as to develop meaningful predictive biomarkers. Interestingly, almost all predictive metabolites ($n = 9/10$) were VLCFA-containing lipids. While our study was purely observational, we hypothesize that the association between VLCFAs and successful immune checkpoint inhibition is based on the impact of T cell metabolism.

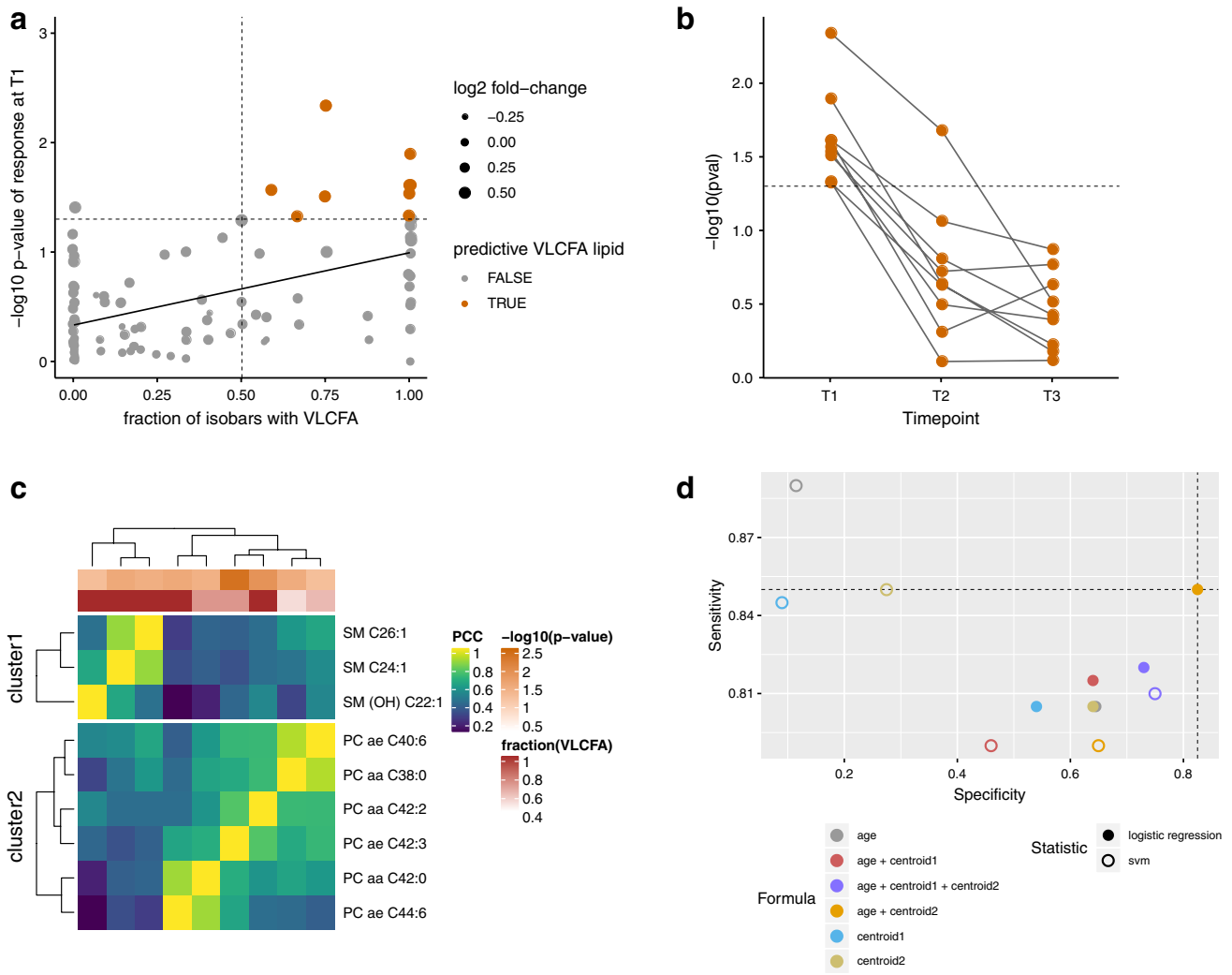

Fig. 3 Predictive modeling. **a** Scatterplot of fraction of potential isobars containing VLCFAs calculated for every lipid in the dataset over the *p* value of the response to immunotherapy (−log10). Nine VLCFA-containing lipids were identified to be predictive at time point 1 ($p < 0.05$). **b** Association of these nine VLCFA-containing lipids with immunotherapy response at T1, T2, and T3. **c** Fraction of potential isobars with VLCFA over the length of the two fatty acids of all measured uGPLs. Linear regression fit with confidence interval ($r = 0.9$). **d** Correlation heatmap for the nine predictive VLCFA-containing lipids. The two clusters comprise sphingomyelins (SMs; cluster 1) and phosphatidylcholines (PCs; cluster 2). **e** ROC statistics of predictive modeling. In total, the predictive performance of six models was tested by applying a tenfold cross validation, which was repeated ten times, for each model. Both a linear (logistic regression) and a non-linear (support vector machine; svm) approach was carried out

Interestingly, this appears to be an early requirement for initiation of the immune response, as only baseline levels (prior to starting immunotherapy) were important in response prediction.

An alteration in lipid composition (e.g. long-chain and very long-chain FA levels) and saturation in tumor tissues compared to healthy tissue or serum has been described [27–29]. Some of these lipids may be biomarkers for cancer risk or development. Since many lipids play a significant role in cancer progression, they are also potential targets for therapeutic intervention. Whether the lipid profiles we measured in this study are directly related to a specific tumor microenvironment (i.e. immuno-permissive vs. immunosuppressive) requires further examination.

Metabolic challenges in the tumor microenvironment, including hypoglycemia and hypoxia, might lead to exhaustion of tumor infiltrating T lymphocytes (TILs). It has been demonstrated that TILs can overcome these constraints by PPARα signaling, which reprograms the metabolic phenotype of TILs to fatty acid catabolism [30]. The authors further demonstrated that PPARα agonists restore the antitumor effects of TILs in a melanoma model. We propose a similar mechanism for the protection of lymphocytes in the blood of tumor patients (Fig. 4a). Myeloid-derived suppressor

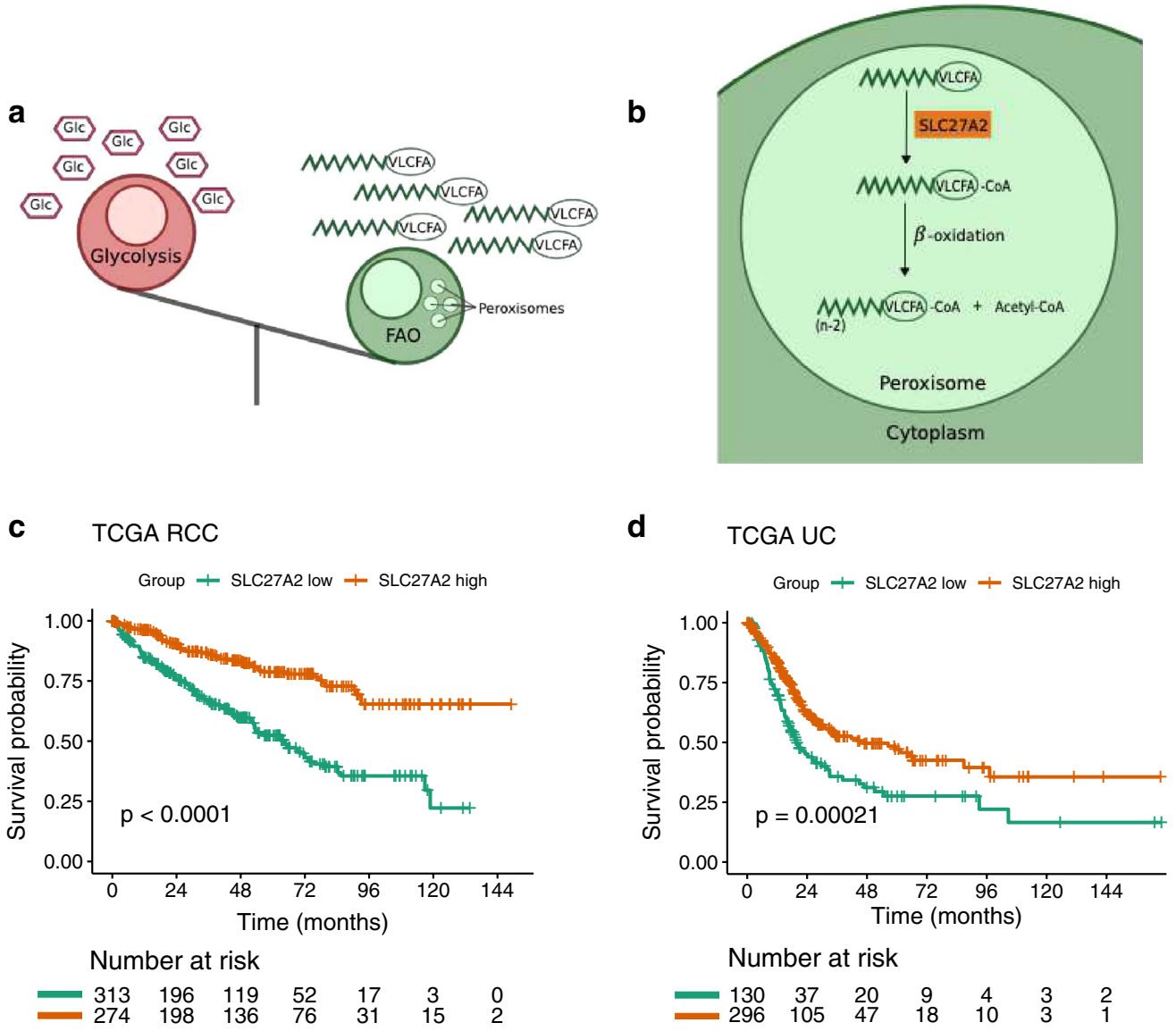

Fig. 4 Proposed mechanism of VLCFA-driven metabolic reprogramming of tumor infiltrating lymphocytes and degradation through SLC27A2. **a** Model: tumor-infiltrating lymphocytes were shown to be metabolically reprogrammed by peroxisome-mediated metabolism of VLCFAs inducing fatty acid oxidation (FAO). In contrast, T cells supplied with glucose (Glc) mainly perform glycolysis [30]. **b**. Activation and degradation of VLCFAs in the peroxisome. VLCFAs are activated by acyl-CoA synthetase SLC27A2 through thioesterification. Degradation of VLCFAs occurs via the chain-shortening peroxisomal β-oxidation pathway. **c** Kaplan–Meier curve of overall survival in clear cell renal cell carcinomas (RCC) stratified by SLC27A2 expression. **d** Kaplan–Meier curve of overall survival in bladder urothelial carcinoma (UC) stratified by SLC27A2 expression

cells [31] and anti-inflammatory type II macrophages [32, 33] within the tumor microenvironment are fueled by the ß-oxidation of lipids, rather than glycolysis. Hence, patients with lower serum VLCFA levels may harbor tumors with a high-VLCFA consumption rate, which reflects their highly immunosuppressive tumor microenvironment (TME). Further studies should examine the metabolome within the tumor as well as the phenotypic characterization of immune cells invading the tumor and the expression of checkpoint inhibitors, e.g. PD-L1, within the TME.

We investigated the expression of the six acyl-CoA synthetases that metabolize VLCFAs (SLC27A2), as a first attempt to understand the impact of a high abundance of VLCFA within the tumor microenvironment. Intriguingly, high expression of SLC27A2 synthetases was of high prognostic value in both the TCGA RCC and UC cohorts. However, further validation is needed with regards to relating mRNA expression values of enzymes to metabolite pools.

The best predictive result in the present study was achieved by combining patient age and a centroid of

VLCFA-containing lipids prior to the first immunotherapy dose (sensitivity: 0.850, specificity: 0.825, ROC: 0.935). Despite a low number of patients, we employed statistical techniques (repeated tenfold cross validation) to avoid overfitting in our cohort.

Further prospective studies using a larger patient cohort are warranted to confirm these findings. In light of our results, we envision that nutritionally supplementing patients with low VLCFA serum levels with VLCFA-containing lipids before starting immunotherapy might help to metabolically reprogram TILs. Prospective studies should investigate if this interesting approach can help to convert immunotherapy non-responders into responders.

Author contributions Conception of the work: SZ, CG; funding acquisition: CG, DJ; sample collection and processing: RK, EC, MJ, AM; metabolomic analysis: MS, BW, AM; data collection and data analysis: AM, SZ, CG, CH; manuscript writing/editing: AM, SZ, GC; critical revision of the manuscript: DJ, MS, BW, RK, RK, EB, MJ; final approval: all the authors.

Funding The National Center for Tumor Diseases (NCT) is supported by the German Cancer Research Center (DKFZ), the University Hospital Heidelberg in cooperation with the Medical Faculty Heidelberg, and by the German Cancer Aid (Deutsche Krebshilfe). This project was supported by the NCT Elevator Pitch 2015.

Compliance with ethical standards

Conflict of interest Matthias Scheffler and Barbara Wolf are employed by BIOCRATES Life Sciences AG. The other authors have declared no competing interests.

Ethical approval and ethical standards The ethics committee of the University of Heidelberg, Germany approved the study design (S023/2016). All procedures performed in studies involving human participants were in accordance with the ethical standards of the institutional and/or national research committee and with the 1964 Helsinki Declaration and its later amendments or comparable ethical standards.

Informed consent All patients provided written informed consent. Informed consent included the permission to take blood samples for research purposes and the use of their anonymized clinical data. Any patient identifiable information was excluded from further sample handling and data processing.

References

1. Astarita G, Langridge J (2013) An emerging role for metabolomics in nutrition science. J Nutr Nutr 6(4–5):181–200
2. Pavlova NN, Thompson CB (2016) The Emerging Hallmarks of Cancer Metabolism. Cell Metab 23(1):27–47
3. Zhu A, Lee D, Shim H (2011) Metabolic positron emission tomography imaging in cancer detection and therapy response. Semin Oncol. https://doi.org/10.1053/j.seminoncol.2010.11.012
4. Hakimi AA, Reznik E, Lee CH et al (2016) An integrated metabolic atlas of clear cell renal cell carcinoma. Cancer Cell. https://doi.org/10.1016/j.ccell.2015.12.004
5. Li B, Qiu B, Lee DSM et al (2014) Fructose-1,6-bisphosphatase opposes renal carcinoma progression. Nature. https://doi.org/10.1038/nature13557
6. Sahu D, Lotan Y, Wittmann B et al (2017) Metabolomics analysis reveals distinct profiles of nonmuscle-invasive and muscle-invasive bladder cancer. Cancer Med. https://doi.org/10.1002/cam4.1109
7. Nizioł J, Bonifay V, Ossoliński K et al (2018) Metabolomic study of human tissue and urine in clear cell renal carcinoma by LC-HRMS and PLS-DA. Anal Bioanal Chem. https://doi.org/10.1007/s00216-018-1059-x
8. Fritsche KL (2015) The science of fatty acids and inflammation. Adv Nutr. https://doi.org/10.3945/an.114.006940
9. Parisi LR, Li N, Atilla-Gokcumen GE (2017) Very long chain fatty acids are functionally involved in necroptosis. Cell Chem Biol. https://doi.org/10.1016/j.chembiol.2017.08.026
10. Sonoda J, Pei L, Evans RM (2008) Nuclear receptors: decoding metabolic disease. FEBS Lett 582(1):2–9
11. Prado-García H, Sánchez-García J (2017) Editoral: immunometabolism in tumor microenvironment. Front Immunol 8:374
12. Haas R, Smith J, Rocher-Ros V et al (2015) Lactate regulates metabolic and proinflammatory circuits in control of T cell migration and effector functions. PLoS Biol. https://doi.org/10.1371/journal.pbio.1002202
13. Lyssiotis CA, Kimmelman AC (2017) Metabolic interactions in the tumor microenvironment. Trends Cell Biol 27(11):863–875
14. Balar AV, Castellano D, O'Donnell PH et al (2017) First-line pembrolizumab in cisplatin-ineligible patients with locally advanced and unresectable or metastatic urothelial cancer (KEYNOTE-052): a multicentre, single-arm, phase 2 study. Lancet Oncol. https://doi.org/10.1016/S1470-2045(17)30616-2
15. Teng F, Meng X, Kong L, Yu J (2018) Progress and challenges of predictive biomarkers of anti PD-1/PD-L1 immunotherapy: a systematic review. Cancer Lett 414:166–173
16. Yarchoan M, Hopkins A, Jaffee EM (2017) Tumor mutational burden and response rate to PD-1 inhibition. N Engl J Med 377(25):2500–2501
17. Galon J, Costes A, Sanchez-Cabo F et al (2006) Type, density, and location of immune cells within human colorectal tumors predict clinical outcome. Science. https://doi.org/10.1126/science.1129139
18. Giannakis M, Li H, Jin C et al (2017) Metabolomic correlates of response in nivolumab-treated renal cell carcinoma and melanoma patients. J Clin Oncol 35:3036
19. Johnson CH, Spilker ME, Goetz L et al (2016) Metabolite and microbiome interplay in cancer immunotherapy. Cancer Res 76(21):6146–6152
20. Schmerler D, Neugebauer S, Ludewig K et al (2012) Targeted metabolomics for discrimination of systemic inflammatory disorders in critically ill patients. J Lipid Res. https://doi.org/10.1194/jlr.P023309
21. Tomas L, Edsfeldt A, Mollet IG et al (2018) Altered metabolism distinguishes high-risk from stable carotid atherosclerotic plaques. Eur Heart J. https://doi.org/10.1093/eurheartj/ehy124
22. Ramos M (2019) CuratedTCGAData: curated data from the Cancer Genome Atlas (TCGA) as multiassayexperiment objects. R package version 1.6.0
23. Thorsson V, Gibbs DL, Brown SD et al (2018) The immune landscape of cancer. Immunity. https://doi.org/10.1016/j.immuni.2018.03.023
24. Pinheiro J, Bates D, DebRoy S (2019) Nlme: linear and nonlinear mixed effects models. In: R package version 3.1-141
25. Betof AS, Nipp RD, Giobbie-Hurder A et al (2017) Impact of age on outcomes with immunotherapy for patients with melanoma. Oncologist. https://doi.org/10.1634/theoncologist.2016-0450

26. Maia MC, Almeida L, Bergerot PG et al (2018) Relationship of tumor mutational burden (TMB) to immunotherapy response in metastatic renal cell carcinoma (mRCC). J Clin Oncol. https://doi.org/10.1200/jco.2018.36.6_suppl.662
27. Halczy-Kowalik L, Drozd A, Stachowska E et al (2019) Fatty acids distribution and content in oral squamous cell carcinoma tissue and its adjacent microenvironment. PLoS One. https://doi.org/10.1371/journal.pone.0218246
28. Paul A, Kumar S, Raj A et al (2018) Alteration in lipid composition differentiates breast cancer tissues: a 1 H HRMAS NMR metabolomic study. Metabolomics. https://doi.org/10.1007/s11306-018-1411-3
29. Pakiet A, Kobiela J, Stepnowski P et al (2019) Changes in lipids composition and metabolism in colorectal cancer: a review. Lipids Health Dis 18(1):29
30. Zhang Y, Kurupati R, Liu L et al (2017) Enhancing CD8 + T cell fatty acid catabolism within a metabolically challenging tumor microenvironment increases the efficacy of melanoma immunotherapy. Cancer Cell. https://doi.org/10.1016/j.ccell.2017.08.004
31. Yan D, Adeshakin AO, Xu M et al (2019) Lipid metabolic pathways confer the immunosuppressive function of myeloid-derived suppressor cells in tumor. Front Immunol. https://doi.org/10.3389/fimmu.2019.01399
32. Namgaladze D (1861) Brüne B (2016) Macrophage fatty acid oxidation and its roles in macrophage polarization and fatty acid-induced inflammation. Biochim Biophys Acta 1861(11):1796–1807
33. Zhang Q, Wang H, Mao C et al (2018) Fatty acid oxidation contributes to IL-1β secretion in M2 macrophages and promotes macrophage-mediated tumor cell migration. Mol Immunol. https://doi.org/10.1016/j.molimm.2017.12.011